COMPUTER RESEARCH AND MODELING
2023 VOL. 15 NO. 3 P. 527–541
DOI: 10.20537/2076-7633-2023-15-3-527-541

КиМ

NUMERICAL METHODS AND THE BASIS FOR THEIR APPLICATION

UDC: 004.93

Image noise removal method based on nonconvex total generalized variation and primal-dual algorithm

C. T. Pham[1,a], T. T. T. Tran[2], H. P. Dang[1]

[1]The University of Danang — University of Science and Technology,
54 Ngyen Luong Bang st., Danang, 550000, Vietnam
[2]The University of Danang — University of Economics,
71 Ngu Hanh Son st., Danang, 550000, Vietnam

E-mail: [a] pcthang@dut.udn.vn (corresponding author)

Received 01.03.2023, after completion — 23.03.2023.
Accepted for publication 10.05.2023.

In various applications, i. e., astronomical imaging, electron microscopy, and tomography, images are often damaged by Poisson noise. At the same time, the thermal motion leads to Gaussian noise. Therefore, in such applications, the image is usually corrupted by mixed Poisson – Gaussian noise.

In this paper, we propose a novel method for recovering images corrupted by mixed Poisson – Gaussian noise. In the proposed method, we develop a total variation-based model connected with the nonconvex function and the total generalized variation regularization, which overcomes the staircase artifacts and maintains neat edges.

Numerically, we employ the primal-dual method combined with the classical iteratively reweighted l_1 algorithm to solve our minimization problem. Experimental results are provided to demonstrate the superiority of our proposed model and algorithm for mixed Poisson – Gaussian removal to state-of-the-art numerical methods.

Keywords: total variation, image restoration, mixed noise, minimization method

Citation: *Computer Research and Modeling*, 2023, vol. 15, no. 3, pp. 527–541.

Pham Cong Thang (corresponding author) would like to express his very great appreciation to colleagues at IT Faculty, DUT, for their valuable and constructive comments during this research work. This work is supported by The Murata Science Foundation and The University of Danang — University of Science and Technology, code number of Project T2021-02-03MSF.

1. Introduction

Image denoising is an important step in various applications such as astronomical imaging, electron microscopy, tomography [Brune, Sawatzky, Burger, 2011; Okawa et al., 2012; Cesarelli et al., 2013; Mevenkamp et al., 2015; Zhang, Song, Dai, 2017]. In these applications, image sensors measure scene irradiance by counting the number of photons coming on the sensor. The independent events of photon detections follow a random distribution. The uncertainty described by this distribution is known as photon noise, also known as Poisson noise [Hasinoff, 2014; Pham et al., 2019]. Besides, the thermal motion of charges inside the system leads to thermal noise, which is present in all electrical circuits and increases with temperature. Practically, thermal noise is often modelled as an additive white Gaussian noise [Ott, 1976]. Therefore, the mixed Poisson – Gaussian noise can obviously express the noise present in these imaging applications. [Benvenuto et al., 2008; Chouzenoux et al., 2015].

With growing interest in the Poisson – Gaussian noise model, there exist many methods of image denoising of images under Poisson – Gaussian noise, for instance, the simplified noise model [Jeong et al., 2014], Variance Stabilization [Bohra et al., 2019], exact Poisson – Gaussian likelihood [Chouzenoux et al., 2015], blindspot neural network [Khademi et al., 2021], total variation (TV) based methods [Calatroni, De Los Reyes, Schronlieb, 2017], Anscombe transformation [Makitalo, Foi, 2013], dictionary learning [Zou, Xia, 2018] etc.

In this work, we focus on the TV based method for Poisson – Gaussian noise removal. Under the TV framework, the TV-based mixed Poisson – Gaussian noise removal model is expressed as follows (TV model) [Pham, Tran, Gamard, 2020]:

$$\mathbf{U}^* = \underset{\mathbf{U}}{\operatorname{argmin}} \left(\int_{\mathcal{B}} |\nabla \mathbf{X}| \, dx + \frac{\lambda}{2} \int_{\mathcal{B}} (\mathbf{U} - \mathbf{F})^2 \, dx + \beta \int_{\mathcal{B}} (\mathbf{U} - \mathbf{F} \log \mathbf{U}) \, dx \right), \tag{1}$$

where $\mathbf{F}$ is the noise image; $\mathcal{B} \subset \mathbb{R}^2$ is a bounded open set, $\mathbf{U}$ must be positive over Ω; and λ, β are positive regularization parameters.

The TV regularization framework (1) allows the noise removal well with sharp edges. Unfortunately, it often leads to undesired staircase artifacts in the reconstruction, since it tends to transform the smooth regions of the result into piecewise constant regions during the iterative process. Many modified TV regularizations were proposed to overcome the issue, such as total generalized variation [Bredies, Kunisch, Pock, 2010; Bredies, Dong, Hintermller, 2013; He et al., 2014a], nonlocal total variation [Kayyar, Jidesh, 2018], TV combined with a higher-order term [Lysaker, Tai, 2006; Li et al., 2007], fractional order TV [Chowdhury et al., 2020], overlapping TV [Jon et al., 2021], Euler's elastic model [Zhang et al., 2017], the mean curvature model [Gong, 2019], and so on. In this paper, we focus on the total generalized variation (TGV) regularization which has a superior performance in image reconstruction to TV-based regularization models. The TGV model for mixed Poisson – Gaussian noise removal can be expressed as follows (TGV) [Pham et al., 2021]:

$$\mathbf{U}^* = \underset{\mathbf{U}}{\operatorname{argmin}} \left(TGV_{\alpha}^2(\mathbf{U}) + \frac{\lambda}{2} \int_{\mathcal{B}} (\mathbf{U} - \mathbf{F})^2 \, dx + \beta \int_{\mathcal{B}} (\mathbf{U} - \mathbf{F} \log \mathbf{U}) \, dx \right), \tag{2}$$

where the first term TGV_{α}^2 is the second-order TGV regularization, and the scalar $\alpha = (\alpha_1, \alpha_2)$ is the positive parameter.

The TGV-based model (2) is better than the TV model in suppressing the staircasing effect with superior performance. However, the TGV regularization can blur the details of an image while removing noise, and sometimes even lost some details. To avoid the issue, nonconvex TGV (NC TGV) was designed to further preserve sharp discontinuities and clear details of the image while suppressing

the artifact effect [Zhang et al., 2018; Na et al., 2019]. In this work, we investigate the nonconvex total generalized variation regularization model to remove mixed Poisson – Gaussian noise, which cleverly combines the advantage of TGV regularization with nonconvex penalty as follows:

$$\mathbf{U}^* = \underset{\mathbf{U}}{\operatorname{argmin}} \left(NCTGV_\alpha^2(\mathbf{U}) + \frac{\lambda}{2} \int_\Omega (\mathbf{U} - \mathbf{F})^2 \, dx + \beta \int_\Omega (\mathbf{U} - \mathbf{F} \log \mathbf{U}) \, dx \right), \tag{3}$$

where $NCTGV_\alpha^2$ is the nonconvex form of TGV_α^2, and its definition will be given in the next section.

Our main contributions to this paper are the following. We propose a novel total variation model for recovering images under mixed Poisson – Gaussian noise on the basis of the nonconvex penalty with the TGV regularizer. The second important contribution is a combination of the classical iteratively reweighted l_1 algorithm and primal-dual framework for solving the minimization problem. Finally, in comparison with existing models, experimental results demonstrate significantly better outcomes of our method for image reconstruction than those of compared methods, with respect to image restoration accuracy and visual quality.

The rest of the paper is organized as follows. Section 2 establishes a novel mixed Poisson – Gaussian image denoising model. In Section 3, we propose an alternating minimization method for solving the minimization problem. We present some reconstruction results of our proposed method and compare them with the results obtained by well-known existing methods in Section 4. Finally, some conclusions are given in Section 5.

2. The Proposed model

The concept of the second-order TGV is introduced in [Bredies, Kunisch, Pock, 2010; Bredies, Dong, Hintermller, 2013], thus omitted. According to [Bredies, Kunisch, Pock, 2010; Bredies, Dong, Hintermller, 2013], the discrete TGV_α^2 regularization of $\mathbf{U}$ can be formulated as

$$TGV_\alpha^2(\mathbf{U}) = \min_{\mathbf{M}} \alpha_1 \|\nabla \mathbf{U} - \mathbf{M}\|_1 + \alpha_2 \|\mathcal{E}(\mathbf{M})\|_1, \tag{4}$$

where $\mathbf{M} = (\mathbf{M}_1, \mathbf{M}_2)^T$, $\mathcal{E}(\mathbf{M}) = \frac{1}{2}\left(\nabla \mathbf{M} + \nabla \mathbf{M}^T\right)$.

The operators $\mathcal{E}(\mathbf{M})$ and $\nabla \mathbf{U}$ can be defined as follows:

$$\nabla \mathbf{U} = \begin{bmatrix} \nabla_1 \mathbf{U} \\ \nabla_2 \mathbf{U} \end{bmatrix} \quad \text{and} \quad \mathcal{E}(\mathbf{M}) = \begin{bmatrix} \nabla_1 \mathbf{M}_1 & \frac{1}{2}(\nabla_2 \mathbf{M}_1 + \nabla_1 \mathbf{M}_2) \\ \frac{1}{2}(\nabla_2 \mathbf{M}_1 + \nabla_1 \mathbf{M}_2) & \nabla_2 \mathbf{M}_2 \end{bmatrix}, \tag{5}$$

where $\nabla = (\nabla_1; \nabla_2)$, ∇_1 and ∇_2 are derivative operators in the horizontal and vertical directions, respectively.

Using nonconvex potential function in the TGV_α^2 regularization (4), the nonconvex regularization is described as

$$NCTGV_\alpha^2(\mathbf{U}) = \min_{\mathbf{M}} \left(\alpha_1 \Phi(\|\nabla \mathbf{U} - \mathbf{M}\|_1) + \alpha_2 \Phi(\|\mathcal{E}(\mathbf{M})\|_1) \right), \tag{6}$$

where Φ is a nonconvex potential function.

In this paper, we introduce a nonconvex potential function $\Phi(|q|) = (|q| + \epsilon)^s$, $0 < s < 1$, $\epsilon > 0$. From (3), (4), and (6), we propose a novel NCTGV regularized model for mixed Poisson – Gaussian noise removal as follows (NCTGV model):

$$\min_{\mathbf{U},\mathbf{M}} \left(\alpha_1 \Phi(\|\nabla \mathbf{U} - \mathbf{M}\|_1) + \alpha_2 \Phi(\|\mathcal{E}(\mathbf{M})\|_1) + \frac{\lambda}{2}(\mathbf{U} - \mathbf{F})^2 + \beta \langle 1, \, \mathbf{U} - \mathbf{F} \log \mathbf{U} \rangle \right). \tag{7}$$

Using the iteratively reweighted l_1 algorithm [Candes, Wakin, Boyd, 2008], we construct (7) to the following convex approximation:

$$\min_{\mathbf{U},\mathbf{M}}\left(\alpha_1\omega_1^{(k)}(\|\nabla\mathbf{U}-\mathbf{M}\|_1)+\alpha_2\omega_2^{(k)}(\|\mathcal{E}(\mathbf{M}\|_1)++\frac{\lambda}{2}(\mathbf{U}-\mathbf{F})^2+\beta\langle 1,\ \mathbf{U}-\mathbf{F}\log\mathbf{U}\rangle\right), \tag{8}$$

where $\omega_1^{(k)}$ and $\omega_2^{(k)}$ are two weights calculated in the kth iteration as follows:

$$\omega_1^{(k)}=\frac{s}{\left(\left\|\nabla\mathbf{U}^{(k)}\right\|_1+\epsilon\right)^{s-1}} \quad \text{and} \quad \omega_2^{(k)}=\frac{s}{\left(\left\|\mathcal{E}\left(\mathbf{M}^{(k)}\right)\right\|+\epsilon\right)^{s-1}}.$$

3. Computational method

In this section, we introduce the numerical method for the problem (8) in detail. For solving the aforementioned optimization problem, many effective numerical techniques can be used, for instance, the primal–dual algorithm [Chambolle, 2004; Chambolle, Pock, 2011], the augmented Lagrangian method [He et al., 2014b; Huang, Ng, Wen, 2008; Wang et al., 2008], the split Bregman method [Goldstein, Osher, 2009; Chen, Chen, Xue, 2015], etc. In this paper, we focus on the primal-dual algorithm and employ it to solve our minimization problem (8).

Returning to the variable splitting method [He et al., 2014b; Chen, Chen, Xue, 2015], we introduce the auxiliary variable $\mathbf{Z}$ and take the replacement $\mathbf{Z}=\mathbf{U}$. Thus, solving the minimization problem (8) is to deal with the following constrained optimization problem:

$$\min_{\mathbf{Z},\mathbf{U},\mathbf{M}}\left(\alpha_1\omega_1^{(k)}(\|\nabla\mathbf{U}-\mathbf{M}\|_1)+\alpha_2\omega_2^{(k)}(\|\mathcal{E}(\mathbf{M})\|_1)+\frac{\lambda}{2}(\mathbf{Z}-\mathbf{F})^2+\beta\langle 1,\ \mathbf{Z}-\mathbf{F}\log\mathbf{Z}\rangle\right),\ \text{s.t. } \mathbf{Z}=\mathbf{U}. \tag{9}$$

The above problem can be converted into the unconstrained minimization problem as follows:

$$\left(\mathbf{Z}^{(k+1)},\ \mathbf{U}^{(k+1)},\ \mathbf{M}^{(k+1)}\right)=\min_{\mathbf{Z},\mathbf{U},\mathbf{M}}\left(\omega_1\gamma_1^{(k)}(\|\nabla\mathbf{U}-\mathbf{M}\|_1)+\alpha_2\omega_2^{(k)}(\|\mathcal{E}(\mathbf{M})\|_1)+\right.$$
$$\left.+\frac{\lambda}{2}(\mathbf{Z}-\mathbf{F})^2+\beta\langle 1,\ \mathbf{Z}-\mathbf{F}\log\mathbf{Z}\rangle+\frac{\theta}{2}\|\mathbf{Z}-\mathbf{U}-\mathbf{b}\|_2^2\right), \tag{10}$$

where $\mathbf{b}^{(k+1)}=\mathbf{b}^{(k)}+\left(\mathbf{U}^{(k+1)}-\mathbf{Z}^{(k+1)}\right)$.

Hence, we obtain

$$\begin{cases}\left(\mathbf{U}^{(k+1)},\ \mathbf{M}^{(k+1)}\right)=\underset{\mathbf{U},\mathbf{M}}{\operatorname{argmin}}\left(\alpha_1\omega_1^{(k)}(\|\nabla\mathbf{U}-\mathbf{M}\|_1)+\alpha_2\omega_2^{(k)}(\|\mathcal{E}(\mathbf{M})\|_1)+\frac{\theta}{2}\left\|\mathbf{Z}^{(k)}-\mathbf{U}-\mathbf{b}^{(k)}\right\|_2^2\right),\\ \mathbf{Z}^{(k+1)}=\underset{\mathbf{Z}}{\operatorname{argmin}}\left(\frac{\lambda}{2}(\mathbf{Z}-\mathbf{F})^2+\beta\langle 1,\ \mathbf{Z}-\mathbf{F}\log\mathbf{Z}\rangle+\frac{\theta}{2}\left\|\mathbf{Z}-\mathbf{U}^{(k+1)}-\mathbf{b}^{(k)}\right\|_2^2\right),\\ \mathbf{b}^{(k+1)}=\mathbf{b}^{(k)}+\left(\mathbf{U}^{(k+1)}-\mathbf{Z}^{(k+1)}\right).\end{cases} \tag{11}$$

To optimize the subproblems $\mathbf{U}$ and $\mathbf{M}$ in (11), we employ the primal–dual algorithm [Esser, Zhang, Chan, 2010; Chambolle, Pock, 2011], which was used for a variety of convex optimization problems appearing in image processing. Under the Legendre – Fenchel transform [Rockafellar, 1970], the minimization problem can be expressed equivalently by the following convex concave saddle-point problem:

$$\min_{\mathbf{U},\mathbf{M}}\max_{\mathbf{p}\in\mathbf{P},\mathbf{q}\in\mathbf{Q}}\left(\langle\nabla\mathbf{U}-\mathbf{M},\ p\rangle+\langle\mathcal{E}(\mathbf{M}),\ \mathbf{q}\rangle+\frac{\theta}{2}\left\|\mathbf{Z}-\mathbf{U}^{(k)}-\mathbf{b}^{(k)}\right\|_2^2\right),$$

where $\mathbf{p}$ and $\mathbf{q}$ stand for two dual variables. The corresponding feasible sets $\mathbf{P}$ and $\mathbf{Q}$ associated with these variables are defined as

$$\mathbf{P} = \left\{\mathbf{p} = (p_1,\ p_2)^T \mid \|\mathbf{p}\|_\infty \leqslant \alpha_1 \omega_1^{(k)}\right\},$$
$$\mathbf{Q} = \left\{\mathbf{q} = \begin{pmatrix} q_{11} & q_{12} \\ q_{21} & q_{22} \end{pmatrix} \mid \|\mathbf{q}\|_\infty \leqslant \alpha_2 \omega_2^{(k)}\right\}.$$

Subsequently, using the projection algorithm, the solutions for the dual variables $\mathbf{p}$ and $\mathbf{q}$ can be found as follows:

$$\mathbf{p}^{(k+1)} = \frac{\mathbf{p}^{(k)} + \zeta\left(\nabla\widetilde{\mathbf{U}}^{(k)} - \widetilde{\mathbf{M}}^{(k)}\right)}{\max}\left(1,\ \frac{\left|\mathbf{p}^{(k)} + \zeta\left(\nabla\widetilde{\mathbf{U}}^{(k)} - \widetilde{\mathbf{M}}^{(k)}\right)\right|}{\alpha_1\omega_1^{(k)}}\right), \tag{12}$$

$$\mathbf{q}^{(k+1)} = \frac{\mathbf{q}^{(k)} + \zeta\mathcal{E}\left(\widetilde{\mathbf{M}}^{(k)}\right)}{\max}\left(1,\ \frac{\left|\mathbf{q}^{(k)} + \zeta\mathcal{E}\left(\widetilde{\mathbf{M}}^{(k)}\right)\right|}{\alpha_2\omega_2^{(k)}}\right), \tag{13}$$

where ζ is a step parameter.

The minimization problem for the primal variable $\mathbf{U}$ has the following form:

$$\min_{\mathbf{U}}\left(\left\langle\nabla\mathbf{U},\ \mathbf{p}^{(k+1)}\right\rangle + \frac{\theta}{2}\left\|\mathbf{U} - \mathbf{Z}^{(k)} + \mathbf{b}^{(k)}\right\|_2^2\right). \tag{14}$$

Based on the discrete divergence operator [Esser, Zhang, Chan, 2010], we transform the problem (14) to the following minimization problem:

$$\min_{\mathbf{U}}\left(-\left\langle\mathbf{U},\ \operatorname{div}\mathbf{p}^{(k+1)}\right\rangle + \frac{\theta}{2}\left\|\mathbf{U} - \mathbf{Z}^{(k)} + \mathbf{b}^{(k)}\right\|_2^2\right), \tag{15}$$

where $\operatorname{div}\mathbf{p}^{(k+1)} = \left(\nabla_1 p_1^{(k+1)} + \nabla_2 p_2^{(k+1)}\right)$.

Using the gradient descent method, the solution of $\mathbf{U}$ in (15) can be identified as

$$\mathbf{U}^{(k+1)} = \mathbf{U}^{(k)} - \tau\left(-\operatorname{div}\mathbf{p}^{(k+1)} + \theta\left(\mathbf{U}^{(k+1)} - \mathbf{Z}^{(k)} + \mathbf{b}^{(k)}\right)\right).$$

Hence, we obtain

$$\mathbf{U}^{(k+1)} = \frac{\mathbf{U}^{(k)} + \tau\left(\operatorname{div}\mathbf{p}^{(k+1)} + \theta\left(\mathbf{Z}^{(k)} - \mathbf{b}^{(k)}\right)\right)}{1 + \tau\theta}. \tag{16}$$

For the primal variable $\mathbf{M}$, we have the following minimization problem:

$$\min_{\mathbf{M}}\left(\left\langle-\mathbf{M}^{(k)},\ \mathbf{p}^{(k+1)}\right\rangle + \langle\mathcal{E}(\mathbf{M}),\ \mathbf{q}\rangle\right). \tag{17}$$

Similarly, we transform the above problem into the following:

$$\min_{\mathbf{M}}\left(\left\langle-\mathbf{M}^{(k)},\ \mathbf{p}^{(k+1)}\right\rangle - \langle\mathbf{M},\ \operatorname{div}\mathbf{q}\rangle\right), \tag{18}$$

where

$$\operatorname{div}\mathbf{q}^{(k+1)} = \begin{pmatrix} \nabla_1 q_{11}^{(k+1)} + \nabla_2 q_{12}^{(k+1)} \\ \nabla_1 q_{21}^{(k+1)} + \nabla_2 q_{22}^{(k+1)} \end{pmatrix}.$$

We employs the gradient descent method and obtain

$$\mathbf{M}^{(k+1)} = \mathbf{M}^{(k)} - \tau\left(-\operatorname{div}\mathbf{q}^{(k+1)} - \mathbf{p}^{(k+1)}\right). \tag{19}$$

Hence, we have

$$\mathbf{M}^{(k+1)} = \mathbf{M}^{(k)} + \tau\left(\operatorname{div}\mathbf{q}^{(k+1)} + \mathbf{p}^{(k+1)}\right).$$

Following [Esser, Zhang, Chan, 2010; Chambolle, Pock, 2011], the variables $\widetilde{\mathbf{M}}^{(k)}$ and $\widetilde{\mathbf{U}}^{(k)}$ in (12) and (13) can be calculated by

$$\widetilde{\mathbf{M}}^{(k+1)} = 2\mathbf{M}^{(k+1)} - \widetilde{\mathbf{M}}^{(k)},$$
$$\widetilde{\mathbf{U}}^{(k+1)} = 2\mathbf{U}^{(k+1)} - \widetilde{\mathbf{U}}^{(k)}.$$

For the $\mathbf{Z}$ subproblem, the optimality condition reads

$$\lambda(\mathbf{Z} - \mathbf{F}) + \beta\left(\mathbf{1} - \frac{\mathbf{F}}{\mathbf{Z}}\right) + \theta\left(\mathbf{Z} - \mathbf{U}^{(k+1)} - \mathbf{b}^{(k)}\right).$$

We have

$$(\lambda + \theta)\left(\mathbf{Z}^{(k+1)}\right)^2 - \left(\lambda\mathbf{F} - \beta + \theta\mathbf{U}^{(k+1)} + \theta\mathbf{b}^{(k)}\right)\mathbf{Z}^{(k+1)} - \beta\mathbf{F} = 0.$$

The positive solution of $\mathbf{Z}^{(k+1)}$ is given by

$$\mathbf{Z}^{(k+1)} = \frac{\left(\lambda\mathbf{F} - \beta + \theta\mathbf{U}^{(k+1)} + \theta\mathbf{b}^{(k)}\right) + \sqrt{\left(\lambda\mathbf{F} - \beta + \theta\mathbf{U}^{(k+1)} + \theta\mathbf{b}^{(k)}\right)^2 + 4(\lambda + \theta)\beta\mathbf{F}}}{2(\lambda + \theta)}. \tag{20}$$

The complete method is summarized in Algorithm 1.

Algorithm 1. Algorithm for Poisson noise removal

Initialize: $\zeta > 0$ and $\tau > 0$.
$\widetilde{\mathbf{U}}^{(0)} = \mathbf{U}^{(0)} = \mathbf{F}$, $\mathbf{M}^{(0)} = \widetilde{\mathbf{M}}^{(0)} = \nabla\mathbf{U}^{(0)}$, $\mathbf{Z}^{(0)} = \mathbf{U}^{(0)}$; $\mathbf{p}^{(0)} = \mathbf{q}^{(0)} = 0$; $k = 1$
while $\left(\frac{\left\|\mathbf{U}^{(k)} - \mathbf{U}^{(k-1)}\right\|_2}{\left\|\mathbf{U}^{(k)}\right\|_2} < \epsilon\right) \Big\| \, (k \geqslant N_{max})$ **do**
  Compute $\mathbf{p}^{(k+1)}$ by (12)
  Compute $\mathbf{p}^{(k+1)}$ by (13)
  Compute $\mathbf{U}^{(k+1)}$ by (16)
  Compute $\mathbf{M}^{(k+1)}$ by (19)
  Compute $\mathbf{Z}^{(k+1)}$ by (20)
  Update $\widetilde{\mathbf{U}}^{(k+1)} = 2\mathbf{U}^{(k+1)} - \widetilde{\mathbf{U}}^{(k)}$
  Update $\widetilde{\mathbf{M}}^{(k+1)} = 2\mathbf{M}^{(k+1)} - \widetilde{\mathbf{M}}^{(k)}$
  Update $\mathbf{b}^{(k+1)} = \mathbf{b}^{(k)} + \left(\mathbf{U}^{(k+1)} - \mathbf{Z}^{(k+1)}\right)$
  $k = k + 1$
end while
return $\mathbf{U}$

4. Numerical experiments

In this section, we show some numerical results to demonstrate the performance of the proposed model for mixed Poisson – Gaussian noise removal. In order to prove the superiority of the proposed model, we compare our results with closely related approaches: the TV model and the TGV model. The compared models are implemented by the state-of-the-art alternating minimization algorithm. The standard test images are gray scale images House (256×256), Baby (256×256), Brain (256×256), and

Woman (228×344), shown in Figure 1. We stop the iterations of all tested algorithms with tolerance $\epsilon = 0.0001$ or $N_{\max} = 300$. Meanwhile, we take the peak signal-to-noise ratio (PSNR), and the structural similarity index (SSIM) [Bovik, Wang, 2006] for the quantitative evaluation:

$$PSNR = 10\log_{10}\left(\frac{255^2 \cdot MN}{\|X^* - X\|_2^2}\right),$$

$$SSIM(\mathbf{X}, \mathbf{X}^*) = \frac{\left(2\mu_{\mathbf{X}}\mu_{\mathbf{X}^*} + c_1\right)\left(2\sigma_{\mathbf{X},\mathbf{X}^*} + c_2\right)}{\left(\mu_{\mathbf{X}}^2 + \mu_{\mathbf{X}^*}^2 + c_1\right)\left(\sigma_{\mathbf{X}}^2 + \sigma_{\mathbf{X}^*}^2 + c_2\right)},$$

where $\mathbf{X}$, $\mathbf{X}^*$ are the clean image, the restored or observed image, respectively; M and N are the number of image pixels in rows and columns, $\mu_{\mathbf{X}}$, $\mu_{\mathbf{X}^*}$ are the means of $\mathbf{X}$, $\mathbf{X}^*$, respectively; $\sigma_{\mathbf{X}}$, $\sigma_{\mathbf{X}^*}$ their standard deviations; $\sigma_{\mathbf{X},\mathbf{X}^*}$ the covariance of two images $\mathbf{X}$ and $\mathbf{X}^*$; c_1, c_2 are positive constants.

(a) House (b) Lena (c) Brain (d) Woman

Figure 1. Test images

Empirically, all images are processed with the equivalent parameters $\lambda = 0.4$, $\beta = 0.6$ which have given the best restoration results. The compared methods are implemented by their optimal values. The observed images are simulated by Poisson noise with $\varsigma_{\mathcal{P}}$, and by Gaussian noise with standard deviation $\varsigma_{\mathcal{G}}$. The code implementing the suggested algorithm is published on GitHub at https://github.com/pacotha/Non-convex-TGV-for-mixed-noise-removal.

In the first simulation, we show in Figure 2 the results of compared different methods on test images with the noisy level $\varsigma_{\mathcal{P}} = 120$, $\varsigma_{\mathcal{G}} = 5$. Column (a) of Figure 2 denotes corrupted images. Meanwhile, in other columns (b–d) of Figure 2, we present the reconstruction results by the compared methods. Besides, the local zoom-in details of original images, noisy images, and recovered results by different models are separately shown in Figures 3, 4. The quantitative image quality assessments of the compared approaches are also summarized in Table 1. From Figures 2–4 and Table 1, our proposed model provides the best image restoration, visually and quantitatively, in terms of image denoising and edge-preserving as compared to some existing related methods.

Table 1. PSNR and SSIM values for noisy images and restored images with noise level $\varsigma_{\mathcal{P}} = 120$, $\varsigma_{\mathcal{G}} = 5$

Image	PSNR				SSIM			
	Noisy	TV	TGV	Ours	Noisy	TV	TGV	Ours
House	20.4289	27.3594	27.4041	27.8068	0.4826	0.8098	0.8110	0.8216
Lena	20.4289	24.3595	24.7797	25.3585	0.4806	0.8129	0.8204	0.8315
Brain	23.6874	28.9434	29.2155	29.8371	0.6822	0.8713	0.8815	0.8968
Woman	20.2988	28.8955	29.3498	30.3706	0.4527	0.8709	0.8796	0.8957

In the second simulation, we show in Figure 5 the reconstruction results given by the compared methods on test images with the noisy level $\varsigma_{\mathcal{P}} = 120$, $\varsigma_{\mathcal{G}} = 10$. Similarly, column (a) of Figure 5 shows

(a) Noisy (b) TV (c) TGV (d) Ours

Figure 2. Recovered results for the test images with $\varsigma_{\mathcal{P}} = 120$, $\varsigma_{\mathcal{G}} = 5$

observed images. In the other columns (b–d) of Figure 5, we show the image denoising results by the compared methods. We also enlarge recovered results via different models in Figures 6, 7. In these

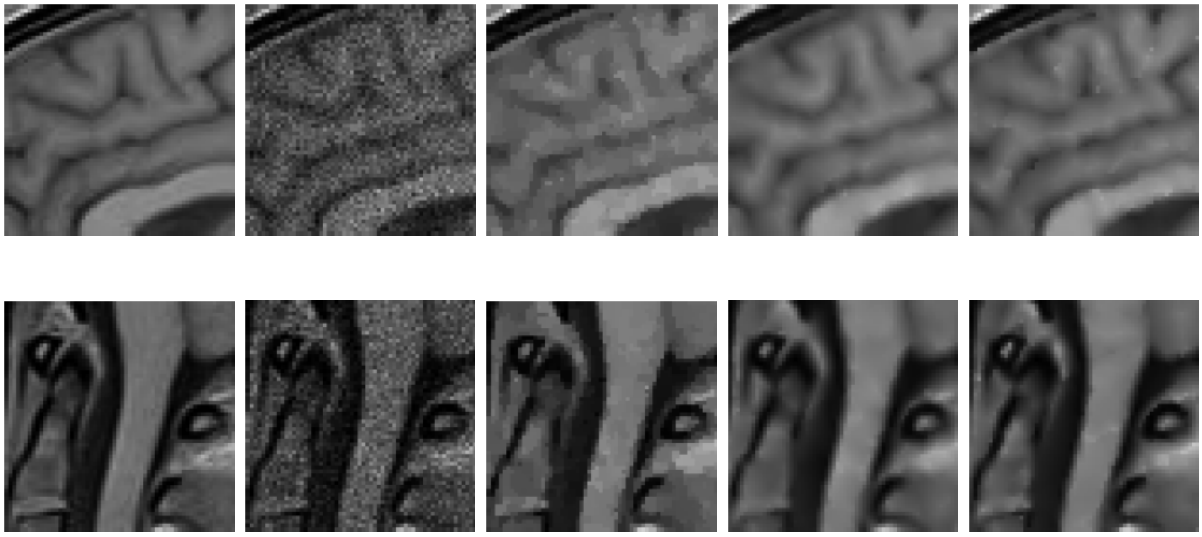

(a) Original (b) Noisy (c) TV (d) TGV (e) Ours

Figure 3. The zoomed-in part of the recovered images in the second row of Figure 2

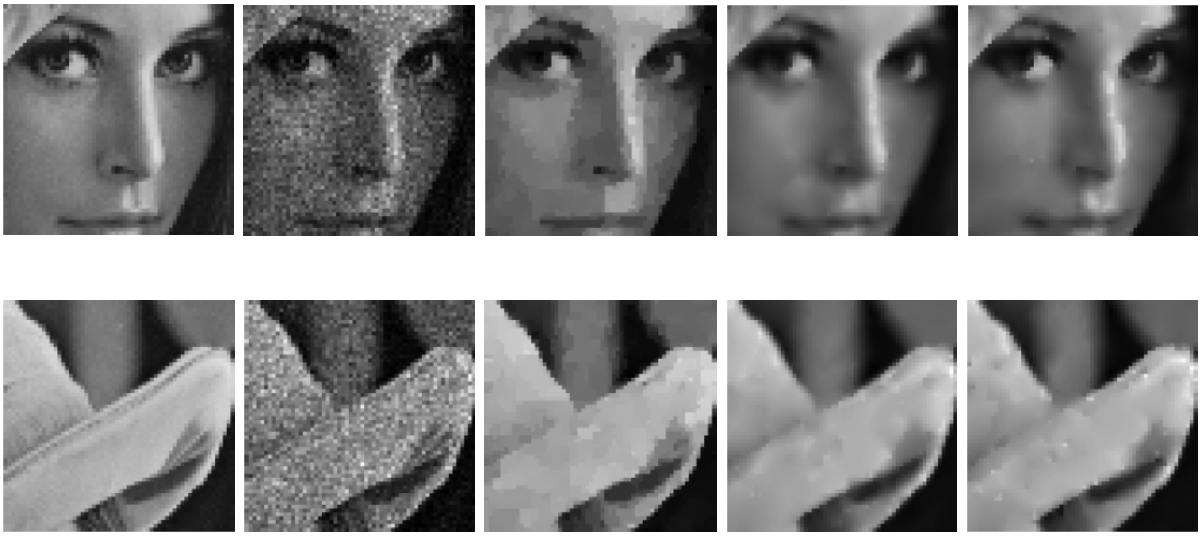

(a) Original (b) Noisy (c) TV (d) TGV (e) Ours

Figure 4. The zoomed-in part of the recovered images in the third row of Figure 2

Figures, we also enlarge the details of original images and observed images. Moreover, the measurable comparisons PSNR and SSIM are detailed in Table 2.

Table 2. PSNR and SSIM values for noisy images and restored images with noise level $\varsigma_{\mathcal{P}} = 120$, $\varsigma_{\mathcal{G}} = 10$

Image	PSNR				SSIM			
	Noisy	TV	TGV	Ours	Noisy	TV	TGV	Ours
House	18.3839	24.9696	25.5657	26.1176	0.3890	0.7715	0.7737	0.7822
Lena	18.9910	23.9098	24.4881	25.0796	0.3683	0.7704	0.7847	0.7971
Brain	20.9437	26.6028	27.4125	27.8851	0.5876	0.8287	0.8508	0.8623
Woman	18.4001	28.1390	28.7557	29.1461	0.3415	0.8437	0.8584	0.8697

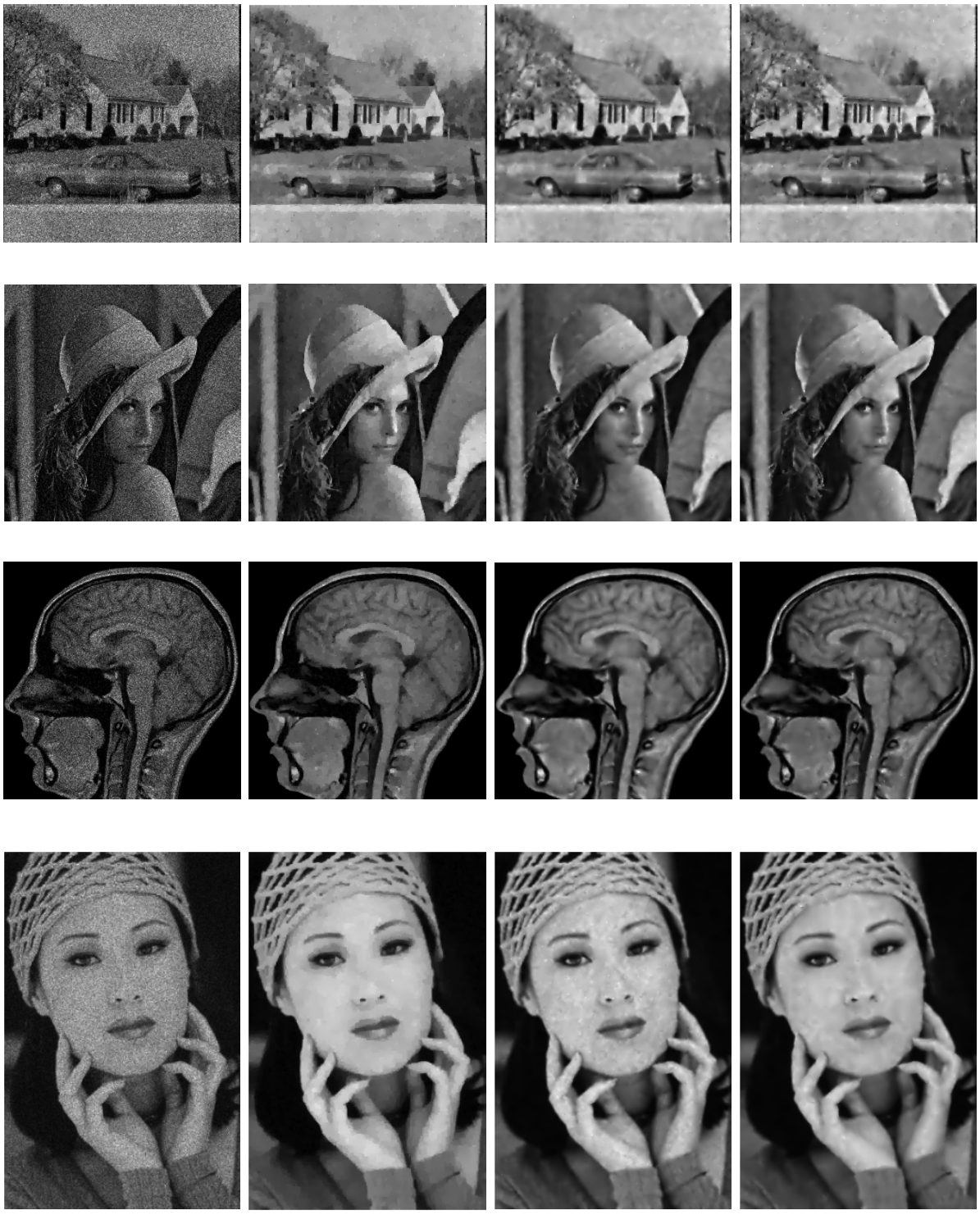

(a) Noisy (b) TV (c) TGV (d) Ours

Figure 5. Recovered results for the test images with $\varsigma_{\mathcal{P}} = 120$, $\varsigma_{\mathcal{G}} = 10$

Finally, we illustrate the capability of our methods for recovering images with the high noise level $\varsigma_{\mathcal{P}} = 60$, $\varsigma_{\mathcal{G}} = 10$. The restored images by three different models are shown in the columns (b–d)

(a) Original (b) Noisy (c) TV (d) TGV (e) Ours

Figure 6. The zoomed-in part of the recovered images in the first row of Figure 5

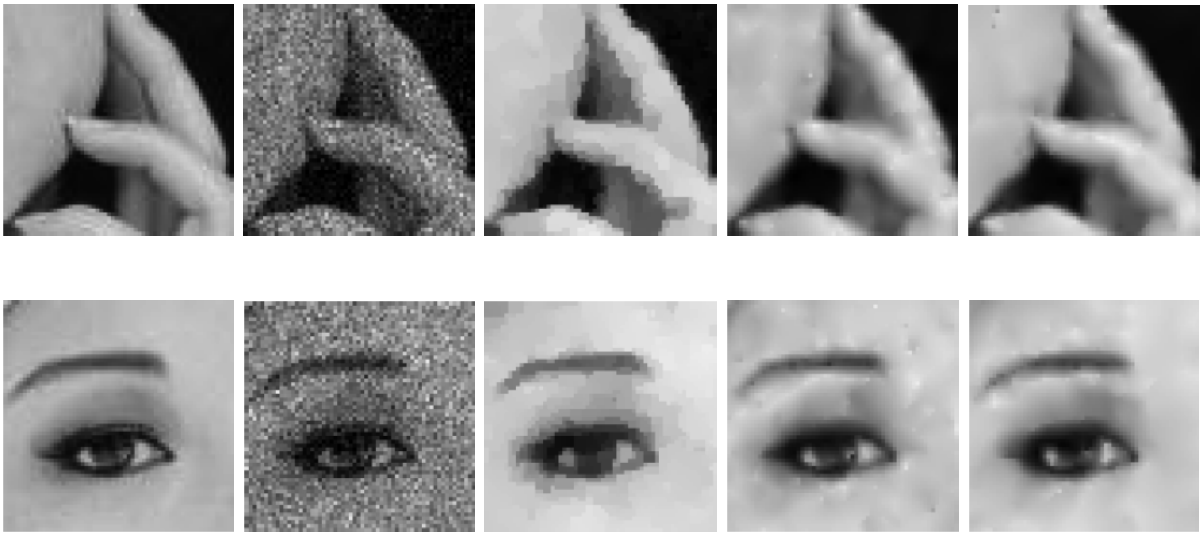

(a) Original (b) Noisy (c) TV (d) TGV (e) Ours

Figure 7. The zoomed-in part of the recovered images in the fourth row of Figure 5

of Figure 8 separately. Subsequently, Table 3 reports the measurable comparisons in terms of the PSNR and SSIM values.

Table 3. PSNR and SSIM values for noisy images and restored images with noise level $\varsigma_{\mathcal{P}} = 60$, $\varsigma_{\mathcal{G}} = 10$

Image	PSNR				SSIM			
	Noisy	TV	TGV	Ours	Noisy	TV	TGV	Ours
House	13.8722	23.4685	23.5466	23.9332	0.2245	0.6776	0.6745	0.6845
Lena	14.3292	22.8149	23.5466	23.9222	0.2007	0.7079	0.7117	0.7203
Brain	15.8037	22.5750	24.3170	25.4661	0.4299	0.7395	0.7628	0.7792
Woman	13.9611	25.3322	25.7857	26.2747	0.1906	0.7392	0.7896	0.8001

(a) Noisy (b) TV (c) TGV (d) Ours

Figure 8. Recovered results for the test images with $\varsigma_{\mathcal{P}} = 60$, $\varsigma_{\mathcal{G}} = 10$

From Figures 2–8, intuitively, our proposed method has the capability of handling the staircase effect and maintaining neat edges. Moreover, the images recovered by our method have fewer artifacts. From Tables 1–3 our method allows for obtaining better measurable restorations then other efficient

methods with the larger PSNR, and SSIM values. Clearly, we can see that our method outperforms the others both in terms of restoration precision and visual quality.

5. Conclusion

In this article, we have investigated a novel variational model connected with the nonconvex function and the total generalized variation regularization. The proposed model is to effectively suppress the staircase effect and maintain neat contours for restoring images degraded by mixed Poisson – Gaussian noise. To obtain the solution to the optimization problem, we employ the alternating method of multipliers connected with the iteratively reweighted l_1 algorithm. Finally, compared with the existing well-known methods, the experiments demonstrate the efficiency of the proposed method.

References

Benvenuto F., Camera A. L., Theys C. et al. The study of an iterative method for the reconstruction of images corrupted by Poisson and Gaussian noise // Inverse Probl. — 2008. — Vol. 24, No. 3. — P. 1–20.

Bredies K., Dong Y., Hintermller M. Spatially dependent regularization parameter selection in total generalized variation models for image restoration // Int. J. Comput. Math. — 2013. — Vol. 90, No. 1. — P. 109–123.

Bredies K., Kunisch K., Pock T. Total generalized variation // SIAM J. Imaging Sci. — 2010. — Vol. 3, No. 3. — P. 492–526.

Brune C., Sawatzky A., Burger M. Primal and dual Bregman methods with application to optical nanoscopy // Int. J. Comput. Vis. — 2011. — Vol. 92, No. 2. — P. 211–229.

Bohra P. et al. Variance-stabilization-based compressive inversion under Poisson or Poisson – Gaussian noise with analytical bounds // Inverse Probl. — 2019. — Vol. 35. — P. 1–38.

Bovik A. C., Wang Z. Modern image quality assessment, synthesis lectures on image, video, and multimedia processing. — Morgan and Claypool Publishers, 2006. — 156 p.

Calatroni L., De Los Reyes J., Schronlieb C. Infimal convolution of data discrepancies for mixed noise removal // SIAM J. Imaging Sci. — 2017. — Vol. 10, No. 3. — P. 1196–1233.

Candes E. J., Wakin M. B., Boyd S. P. Enhancing sparsity by reweighted l_1 minimization // J. Fourier Anal. Appl. — 2008. — Vol. 14, No. 5–6. — P. 877–905.

Cesarelli M., Bifulco P., Cerciello T., Romano M., Paura L. X-ray fluoroscopy noise modeling for filter design // Int. J. Comput. Assist. Radiol. Surg. — 2013. — Vol. 8, No. 2. — P. 269–278.

Chambolle A. An algorithm for total variation minimization and applications // J. Math. Imaging Vis. — 2004. — Vol. 20. — P. 89–97.

Chambolle A., Pock T. A first-order primal-dual algorithm for convex problems with applications to imaging // J. Math. Imaging Vis. — 2011. — Vol. 40. — P. 120–145.

Chen D., Chen Y. Q., Xue D. Fractional-order total variation image denoising based on proximity algorithm // Appl. Math. Comput. — 2015 — Vol. 257. — P. 537–545.

Chouzenoux E., Jezierska A., Pesquet J. C., Talbot H. A convex approach for image restoration with exact Poisson – Gaussian likelihood // SIAM J. Imaging Sci. — 2015. — Vol. 8, No. 4. — P. 2662–2682.

Chowdhury M. R., Zhang J., Qin J., Lou Y. Poisson image denoising based on fractional-order total variation // Inverse Probl. Imaging. — 2020. — Vol. 14, No. 1. — P. 77–96.

Esser E., Zhang X., Chan T. A general framework for a class of first order primal–dual algorithms for convex optimization in imaging science // SIAM J. Imaging Sci. — 2010. — Vol. 3, No. 4. — P. 1015–1046.

Goldstein T., Osher S. The split Bregman method for L_1-regularized problems // SIAM J. Imaging Sci. — 2009. — Vol. 2, No. 2. — P. 323–343.

Gong Y. Mean curvature is a good regularization for image processing // IEEE Trans. Circuits Syst. Video Technol. — 2019. — Vol. 29, No. 8. — P. 2205–2214.

Hasinoff S. W. Photon, poisson noise / Ikeuchi K. (ed.) Computer vision. — Boston, MA: Springer US, 2014. — P. 608–610.

He C., Hu C., Yang X., He H. An adaptive total generalized variation model with augmented Lagrangian method for image denoising // Math. Probl. Eng. — 2014a. — P. 1–11.

He C., Hu C., Zhang W., Shi B. A fast adaptive parameter estimation for total variation image restoration // IEEE Trans. Image Process. — 2014b. — Vol. 23, No. 12. — P. 4954–4967.

Huang Y. M., Ng M. K., Wen Y. W. A fast total variation minimization method for image restoration // Multiscale Model. Sim. — 2008. — Vol. 7, No. 2. — P. 774–795.

Jeong B. G., Kim B. C., Moon Y. H., Eom I. K. Simplified noise model parameter estimation for signal-dependent noise // Signal Process. — 2014. — Vol. 96, Part B. — P. 266–273.

Jon K. et al. Image restoration using overlapping group sparsity on hyper-Laplacian prior of image gradient // Neurocomputing. — 2021. — Vol. 420. — P. 57–69.

Kayyar S. H., Jidesh P. Non-local total variation regularization approach for image restoration under a Poisson degradation // J. Mod. Opt. — 2018. — Vol. 65. — P. 2231–2242.

Khademi W. et al. Self-supervised Poisson – Gaussian denoising // IEEE Winter Conference on Applications of Computer Vision (WACV). — 2021. — P. 2130–2138.

Le T., Chartrand R., Asaki T. A variational approach to constructing images corrupted by Poisson noise // J. Math. Imaging Vis. — 2007. — Vol. 27. — P. 257—263.

Li F. et al. Image restoration combining a total variational filter and a fourth-order filter // J. Vis. Commun. Image Represent. — 2007. — Vol. 18, No. 4. — P. 322–330.

Liu X., Huang L. Total bounded variation-based Poissonian images recovery by split Bregman iteration // Math. Methods Appl. Sci. — 2012. — Vol. 35, No. 5. — P. 520–529.

Lysaker M., Tai X. C. Iterative image restoration combining total variation minimization and a second-order functional // Int. J. Comput. Vis. — 2006. — Vol. 66, No. 1. — P. 5–18.

Makitalo M., Foi A. Optimal inversion of the generalized Anscombe transformation for Poisson – Gaussian noise // EEE Trans. Image Process. — 2013. — Vol. 22, No. 1. — P. 91–103.

Mevenkamp N., Binev P., Dahmen W., et al. Poisson noise removal from high-resolution STEM images based on periodic block matching // Adv. Struct. Chem. Imag. — 2015. — Vol. 1, No. 3. — P. 1–19.

Na H., Kang M. Jung M., Kang M. Nonconvex TGV regularization model for multiplicative noise removal with spatially varying parameters // Inverse Probl. Imaging. — 2019. — Vol. 13. — P. 117–147.

Okawa S., Endo Y., Hoshi Y., Yamada Y. Reduction of Poisson noise in measured time-resolved data for time-domain diffuse optical tomography // Med. Biol. Eng. Comput. — 2012. — Vol. 50, No. 1. — P. 69–78.

Ott H. M. Noise reduction techniques in electronic systems. — New York: Wiley-Interscience, 1976. — 294 p.

Pham C. T., et al. An adaptive algorithm for restoring image corrupted by mixed noise // Cybern. Phys. — 2019. — Vol. 8, No. 2. — P. 73–82.

Pham C. T., Tran T. T. T., Gamard G. An efficient total variation minimization method for image restoration // Informatica. — 2020. — Vol. 31, No. 3. — P. 539–560.

Pham C. T., Tran T. T. T., Nguyen T. C., Vo D. H. Second-order total generalized variation based model for restoring images with mixed Poisson – Gaussian noise // Inf. Control Sys. — 2021. — Vol. 2. — P. 20–32.

Rockafellar R. T. Convex analysis. — Princeton, NJ: Princeton University Press, 1970. — 472 p.

Wang Y., Yang J., Yin W., Zhang Y. A new alternating minimization algorithm for total variation image reconstruction // SIAM J. Imaging Sci. — 2008. — Vol. 1, No. 3. — P. 248–272.

Zhang H. et al. Nonconvex and nonsmooth total generalized variation model for image restoration // Signal Process. — 2018. — Vol. 143. — P. 69–85.

Zhang J., Chen R., Deng C., Wang S. Fast linearized augmented Lagrangian method for Euler's elastica model // Numer. Math. Theor. Meth. Appl. — 2017. — Vol. 10, No. 1. — P. 98–115.

Zhang J., Ma M., Wu Z., Deng C. High-order total bounded variation model and its fast algorithm for Poissonian image restoration // Math. Probl. Eng. — 2019. — Vol. 2019. — P. 1–11.

Zhang J., Wei Z., Xiao L. Adaptive fractional-order multi-scale method for image denoising // J. Math. Imaging Vision. — 2012. — Vol. 43. — P. 39–49.

Zhang Y., Song P., Dai Q. Fourier ptychographic microscopy using a generalized Anscombe transform approximation of the mixed Poisson – Gaussian likelihood // Opt. Express. — 2017. — Vol. 25. — P. 168–179.

Zou C., Xia Y. Bayesian dictionary learning for hyperspectral image super resolution in mixed Poisson – Gaussian noise // Signal Process. Image Commun. — 2018. — Vol. 60. — P. 29–41.